Te(IV) immobilization by siderite: Reaction kinetics, mechanism, and Te isotopic fractionation

Anirban Basu[1], Kathrin Schilling[2]*, Alex N. Halliday[3], Naomi Wasserman[4], Thomas M. Johnson[5]

[1]*Department of Earth Sciences, Royal Holloway, University of London, Egham, TW20 0EX, United Kingdom*

[2]*Department of Environmental Health Sciences, Columbia University Mailman School of Public Health, New York, NY, USA*

[3]*Earth Institute, Columbia University, New York, NY, USA*

[4]*Nuclear and Chemical Sciences Division, Lawrence Livermore National Laboratory, Livermore, CA 94550, USA*

[5]*Department of Geology, University of Illinois at Urbana-Champaign, Champaign, IL, 61820, USA*

*Corresponding author: ks3759@columbia.edu

Keywords: Tellurium, siderite, redox, first-order reaction, Te stable isotopes

Abstract

Mining and industrial use over recent decades have released Te into the environment where it potentially contaminates soils, water supplies and food sources. Therefore, it is important to find ways of removing mobile and bioavailable Te from aqueous environments. We report aqueous Te(IV) removal by siderite at varying Te concentrations (2, 6 and 10 mg mL^{-1} Te(IV)) and pH values (7, 7.9 and 9), together with associated isotope fractionation ($\varepsilon^{130}Te/^{125}Te$). Our results show effective immobilization of Te(IV) that follows pseudo-first order rate kinetics. Formation of magnetite indicates reduction of Te(IV) on siderite surfaces and the formation of Te(0). The overall isotope fractionation (ε) is small (-0.23 ± 0.06‰) providing evidence that it is primarily controlled by adsorption of Te(IV) occurring simultaneously with reduction of Te(IV). Therefore, Te(IV) removal by siderite under mildly reducing ferruginous conditions may be identifiable by the characteristically small isotopic fractionation during both natural attenuation and active remediation. To our knowledge, this is the first study reporting reaction mechanisms of Te(IV) immobilization by an environmentally relevant Fe(II) mineral.

1. Introduction

Demand for tellurium (Te) is increasing. Use of Te in electronics, particularly in solar panels (e.g., Cd-Te thin-film solar cells) and in the metallurgy industry have expanded its economic significance over the last decades (Kavlak, and Graedel, 2013; Watari, 2018). Tellurium has been classified as an energy critical element (Hayes and McCullough, 2018; Watari et al., 2020) and the United States Department of Interior (USDOI) and the United States Geological Survey (USGS) included Te in their "2022 Final list of critical minerals" that play a significant role in the US economy and the national security (US DOI, 2022). Less than 1% of life-end products containing Te (e.g., solar panels) are being recycled (Talens Peiro et al., 2013). In addition, the drawback of the high economic demand of other elements such as copper and gold leads to increasing mining activity and the production of Te-containing waste. During mining processes 90% of Te is lost by extraction and refining and thus released to the environment (Kavlak and Graedel, 2013). Particular regions with abandoned mine tailings and alkaline mine drainage (Wray, 1998; Moreno et al., 2007; Qin et al., 2017; Hayes and Ramos, 2019) and metal refineries (Perkins, 2011) are already impacted by high Te concentrations in soil and water. Major distribution pathways for Te in the environment include atmospheric deposition (Perkins, 2011; Wiklund et al., 2018) and aqueous processes in soils and sediments (Gil-Diaz et al, 2018) which ultimately lead to accumulation in plant-based food sources (Ruiz- de Cenzano et al., 2017, Filippini et al., 2019; Doulgeridou et al., 2020). Critical elements such as Te provide the ingredients for materials necessary for modern civilization and how these elements are distributed and cycled in the Earth is a priority science question identified in the recently published document "A Vision for NSF Earth Sciences 2020-2030: Earth in Time (2020)" (National Academies of Sciences, Engineering, and Medicine 2020, Sovacool et al., 2020).

Tellurium has no known nutritional benefit and any exposure to even low levels may cause acute and chronic health issues (Zannoni et al., 2007). Tellurium occurs in four oxidation states (–II; 0; +IV and +VI), and forms compounds chemically analogous to sulfur and selenium. Tellurite (Te(IV)) is 100 to 1,000 times more toxic than geochemically similar selenite (Taylor, 1999, Kessi et al., 2022, Missen et al., 2022). The toxicity of Te(IV) is up to 10 times higher than that of Te(VI) (Zannoni et al., 2007). Acute toxicity of Te was reported from ingestion of metal-oxidizing solutions that contained substantial

concentrations of Te (Yarema and Curry, 2005; Vij and Hardej, 2016). Despite its high toxicity little is known about total tellurium content for many environmental settings and information about the fate of Te in the environment are scarce particularly how and when reduction of Te oxyanions reduces toxicity and exposure (Filella et al. 2019).

It is imperative to investigate the environmental mobilization and sequestration pathways for the soluble oxidized Te species. Tellurium oxyanions (+IV and +VI) are mobile in aqueous environments due to their high solubility but also adsorb strongly to iron (oxy)hydroxides over a wide pH range (Harada and Takahashi, 2008, Kashiwabara et al., 2014). In sharp contrast, reduced Te species (–II; 0) are less soluble and have therefore lower mobility in the environment and reduced bioavailability than the oxidized species. Chemical reduction and adsorption onto minerals surfaces immobilize Te in the environment (Filella et al., 2019; Missen et al., 2020). Several studies have reported reduction of Te oxyanions by bacteria (Tucker et al., 1962; Baesman et al., 2007; Zannoni et al., 2007; Ramos-Ruiz et al., 2015; Choi et al., 2019), but little is known about naturally occurring abiotic reductants. To date, there is only one study demonstrating efficient sorption and reduction of Te(IV) by iron, in the form of nanoscale zero valent iron (ZVI) (Yu et al., 2018). The reduction of Te(IV) by naturally occurring mineral phases has not been investigated at all. It is critical to know how Te oxyanions are reductively immobilized in nature because Te(IV) retention in soil is low and may result in easier release and migration under suboxic conditions (Qin et al., 2017).

Tellurium stable isotopes may serve as useful tracers of natural processes controlling Te cycling. For similar redox sensitive elements such as Se, Cr and U, stable isotopes have been established as effective indicators of redox-driven cycling and immobilization (Clark and Johnson, 2010; Reinhard et al., 2014; Zhu et al., 2014; Schilling et al., 2015; Basu et al., 2016). Tellurium has eight isotopes. ^{122}Te (contribution to the total elemental mass: 2.6%); ^{123}Te (0.9%); ^{124}Te (4.8%); ^{125}Te (7.1); ^{126}Te (19.0%), ^{128}Te (31.6%) and ^{130}Te (33.7%). The isotopes ^{120}Te, ^{123}Te, ^{128}Te and ^{130}Te are considered radioactive but they are effectively “stable” with for the time-scale of environmental and anthropogenic-driven processes due to their extremely long half-lives of 1×10^{16}, 9.2×10^{16}, 2.2×10^{24} and 7.9×10^{20} years, respectively.

Most studies report data in terms of $^{130}Te/^{125}Te$ (Baesman et al., 2007, Fornadel et al., 2017, 2019, Fehr et al., 2018, Fukami et al., 2022) and fewer studies used $^{128}Te/^{125}Te$ (Fehr et al. 2006), $^{128}Te/^{126}Te$ (Hellmann et al. 2021) and $^{130}Te/^{126}Te$ (Wasserman and Johnson, 2020). Yet, only two studies have been conducted to determine Te isotopic fractionation by microorganisms and aqueous abiotic reductants (Smithers and Krouse, 1968; Baesman et al., 2007). Dissimilatory microbial reduction of Te oxyanions induces ε of –1.95 to –4.0‰, where $\varepsilon = 1000‰ \bullet (\alpha - 1)$; and $\alpha = (^{130}Te/^{125}Te)_{product}/(^{130}Te/^{125}Te)_{reactant}$ (Baesman et al., 2007). Abiotic reduction of Te(IV) by cysteine and sulfite leads to ε of –2.35‰ and –4.40‰, respectively (Smithers and Krouse, 1968; Baesman et al., 2007). Tellurium adsorption experiments show that Te(IV) adsorbed onto goethite is about 0.5‰ isotopically lighter than Te(IV) in solution (Wasserman et al., 2017). Theoretical calculations of Te isotopic equilibrium predict that $^{130}Te/^{125}Te$ of Te(VI) may be up to 4.5‰ heavier than that of Te(IV), and $^{130}Te/^{125}Te$ of Te(IV) may be about 5‰ heavier than that of Te(0) at 25°C (Fornadel et al. 2017). Nothing is known about the Te isotopic fractionation during Te(IV) immobilization caused by naturally occurring minerals in moderately reducing suboxic environments such as reducing groundwaters, waste waters and soil pore waters. Variation of 2‰ for $^{130}Te/^{125}Te$ has been observed in tellurides from hydrothermal ore deposits caused by Te redox cycling (Fornadel et al. 2017, 2019). Wasserman and Johnson (2020) reported a range of 1.5‰ for $^{130}Te/^{125}Te$ in soils and sediments. To trace environmental cycling of Te and develop isotopic proxies, we need a detailed understanding of reaction mechanisms involving immobilization and associated isotopic fractionation.

In this study, we determine the mechanism and kinetics of Te(IV) immobilization by siderite, and associated isotope fractionation. Siderite ($FeCO_3$) is known to immobilize a wide range of inorganic contaminants including U(VI), Cr(VI), and Se(IV) by adsorption and/or reduction (Scheinost and Charlet, 2008; Ithurbide et al., 2009; Basu et al., 2012). Additionally, siderite, often occurring as a slurry of small particles, is one of the most effective minerals at buffering the redox potential in anoxic environments (Jensen et al., 2002; Lee and Wilkin, 2010). We investigated the effect of pH and concentrations on the reaction kinetics and Te isotope fractionation to elucidate the dominant reaction pathway (e.g., adsorption *vs.* reduction). Our experimental Te(IV) concentrations reflect Te

concentration reported for ferromanganese nodules (average ~1 mg/kg Te), black shales (1–10 mg/kg Te) as well as Te contaminated sites (~10mg/kg Te in topsoils) (Baturin, 2012; Perkins, 2011, Hein et al., 2003). We report the effect of pH and Te concentrations on reaction kinetics and isotopic fractionation, and show that surface-mediated reduction of Te(IV) by siderite does not exceed Te isotopic fractionation of 0.1–0.3‰.

2. Methods

2.1 Siderite synthesis. Siderite was prepared under strictly anoxic conditions following a previously described method (Wiesli et al., 2004; Rakshit et al., 2008; Basu et al., 2012). All solutions and suspensions were prepared from deoxygenated double-deionized water (18.2 MΩ • cm). Siderite was synthesized by mixing 30 mL of 0.5 M $FeCl_2 \bullet 4H_2O$ with 30 mL of 0.5 M Na_2CO_3 under an anoxic atmosphere. A very fine-grained greyish white precipitate formed instantaneously. An excess amount of Na_2CO_3 was added to the mixture so that there was no Fe(II) left in the solution. The serum bottle was stirred for 48 hours to complete the reaction. The mineral was then rinsed twice with degassed H_2O to remove NaCl, and then resuspended in 31 mL of degassed H_2O. Siderite concentration of the stock suspension is 112.1 g L^{-1}. Using the same method of synthesis, a recent study has reported a uniform particle of size of ~10 μm and framboidal shape of precipitated siderite (Koo and Kim, 2019).

2.2 Te(IV) experiments with siderite. Anoxic batch experiments with Te(IV) solution were carried out in glass serum bottles with a working solution volume of 50 mL. A solution matrix containing 10mM pH buffer solution (CHES: N-Cyclohexyl-2-aminoethanesulfonic acid and MOPS: 3-(N-Morpholino)propane sulfonic acid) and 0.01 M NaCl was used for the experiments. The experiments were conducted at three pH values (7, 7.9 and 9) covering the pH range of most carbonate-bearing near-surface geochemical environments. The pH solution was adjusted to 7.0 and 7.9 with 0.1 M NaOH and MOPS buffer, and to 9.0 using 0.1 M NaOH and CHES buffer, respectively. We carried out three experiments with initial Te(IV) of 10 mg L^{-1} (high Te), 6 mg L^{-1} (intermediate Te) and 2 mg L^{-1} (low Te) for each pH condition. An aliquot of degassed stock Na_2TeO_3 (~120 mg L^{-1} as Te(IV)) was added to the experimental batch reactors to achieve the targeted initial Te(IV) concentrations. An aliquot of 0.4 mL of anoxic siderite ($FeCO_3$) suspension containing 44.9 mg of siderite was added to each

reactor. The reactors were shaken continuously at 125 rpm on an orbital shaker. For a time series analysis of Te(IV) removal, ~3 mL of sample aliquots were withdrawn at several time intervals using N_2 purged syringes. The reactors were shaken vigorously immediately before sampling to keep siderite particles in suspension during sampling. If the particles are evenly suspended in the solution, the removal of the sample aliquot does not significantly alter the siderite concentration in the remaining suspension. All aliquots were filtered through a 0.2 µm syringe filter and stored at 4°C until further analysis.

2.3 Te concentration and isotope analysis. Tellurium concentrations in the subsamples were measured using a PerkinElmer NexION 350D Quadrupole Inductively Coupled Plasma-Mass Spectrometer (Q-ICP-MS) equipped with an Elemental Scientific (Omaha, USA) prepFAST M5 autosampler and autodiluter and operated with the PerkinElmer Syngistix software. Subsamples were analyzed in a 3 vol.% HNO_3 matrix and iridium (m/z 193) was added as internal standard. External calibration coving a range between 0.1 to 100 ng Te/L was performed in matrix matched 3% vol. HNO_3 and 10 µg Ir/L solutions. Blanks, standards and samples were analyzed at m/z 128 and 130 at a dwell time of 25 ms from a series of 60 sweeps and five replicates. After every 10 samples, standard quality control and calibration blanks were analyzed to evaluate potential memory effects and cross contamination.

Methods for the Te isotope measurements and sample preparation are described by Wasserman and Johnson (2020). In brief, a known mass of ^{120}Te-^{124}Te double spike in the form of Te(IV) was added to the sample aliquot to achieve a sample and spike mixed ^{124}Te:^{130}Te ~1. This allows correction for isotopic fractionation during sample preparation and analysis. Te(IV) was separated from the sample matrix using a two-step anion exchange chromatography procedure. A 10 mL polypropylene column with 1 mL of clean AG1-X8 resin (100-200 mesh, BioRad Laboratories) was conditioned with 15 mL of 4 M HCl. The spiked sample aliquot containing between 40 ng and 100 ng of Te(IV) in 4 M HCl was loaded onto the column. To remove most of the sample matrix the column was rinsed with 10 mL of 4 M HCl. Subsequently Te(IV) was collected by adding 4 mL of 0.1 M HCl. The sample was dried down and Te(IV) was converted to Te(VI) by heating at 110°C for 90 minutes by adding 0.02 M $K_2S_2O_8$. There are potential Sn isobaric interferences on masses 120, 122 and 124. Tin was removed by passing

the sample through an additional column containing 1 mL AG1-X8 and rinsing with 0.1 M HCl (Wasserman and Johnson, 2020). Tin remained on the resin while Te(VI) was eluted. The sample was then reduced in 5 M HCl by heating at 110°C for 2 hours. Prior to isotope analysis, the molarity of the processed sample was adjusted to 4 M HCl.

Tellurium isotope ratios were measured using hydride generation multi-collector inductively coupled mass spectrometry (HR MC-ICP-MS; Nu Plasma Instruments, Wrexham, UK) at the University of Illinois at Urbana-Champaign (USA). The samples were introduced to a custom-built hydride generator at a flow rate of 1.0 ml min^{-1}, reacted with 0.2w% sodium borohydride ($NaBH_4$) in 0.2w% sodium hydroxide to form TeH_2 (Wasserman and Johnson, 2020). This method removes potential isobaric and molecular inferences and also provides higher sensitivity. Samples and standards double spiked with ^{120}Te-^{124}Te facilitated precise correction for instrumental mass bias and samples were measured at signal intensity of 1.2–2 V on ^{130}Te. All measurements were reported in the δ notation and normalized to the international Te standard NIST SRM 3156 as follows:

$$\delta^{130/126}Te\ (‰) = \left(\frac{130Te/126Te_{sample}}{130Te/126Te_{standard}} - 1\right) \times 1000 \quad (1)$$

For better comparison with literature values, $\delta^{130/126}$Te was converted to the more commonly used $^{130/125}$Te notation by multiplying $\delta^{130/126}$Te with 1.25. The uncertainty (2σ) was 0.07‰, calculated as twice the root mean square of seven pairs of duplicate analyses.

2.4 Magnitude of isotopic fractionation (ε). We determined the extent of Te isotope fractionation in our experiments by fitting the experimental data to a Rayleigh distillation model, which requires - (1) the product of the reaction is permanently removed from the system (2) it is closed well-mixed reactor with a progressive unidirectional reaction, and (3) and the fractionation factor as to be constant. As all these conditions were met in our batch experiments, the magnitude of Te isotope fractionation was determined by fitting the measured δ^{130}Te values to the Rayleigh distillation model defined as:

$$\delta^{130}Te_{(t)}(‰) = (\delta^{130}Te_0 + 1000) \times \left(\frac{c_{(t)}}{c_0}\right)^{\alpha-1} - 1000 \quad (2)$$

where *c(t)* and *δ(t)* are the concentration and the isotopic composition of the remaining Te(IV) as a

function of time. The fractionation factor (α) is defined as $\alpha = R_{product}/R_{reactant}$, where R is the measured $^{130}Te/^{125}Te$, and often expressed in terms of ε (‰) where $\varepsilon = 1000‰ \bullet (\alpha - 1)$. The magnitude of isotopic fractionation, ε, was calculated from the corresponding slope of the linear regression of $\ln(\delta^{130}Te + 1000)$ *versus* $\ln(c(t)/c_0)$.

2.5 Characterization of reacted mineral. Bulk solid phase mineralogy of the reaction product was determined using powder X-ray diffraction (XRD), and scanning electron microscopy (SEM) (HITACHI S3000). After the experiments, the remaining volume (~20 mL) was centrifuged, and the supernatant was discarded under anoxic conditions in a glove box. The solid material was dried on glass slides under 96% N_2-4% H_2 environment. The glass slides with dried material were kept under anoxic conditions prior to XRD and SEM analysis. The SEM was equipped with an Aztec energy-dispersive X-ray detection system (EDS) by Oxford Instruments and used an acceleration of 20 kV and 76 μA. The XRD analyses were carried out using a Philips PW1830/3020 diffractometer equipped with alpha Cu Kα radiation. All XRD spectra were background-corrected and analyzed using the profile refinement method by Rietveld (Rietveld, 1969). No semi-quantitative analysis of the XRD data was performed. So, we cannot rule out presence of some Te(IV) as an adsorbed species in the solid phase.

3. Results and discussions

3.1 Kinetics of Te(IV) removal. Aqueous Te(IV) concentration decreases systematically with time in each experiment (Figure 1) caused by the interaction with siderite. About 70% of Te(IV) is removed from solution within the first 7 hours for all tested pH conditions. The total amount of Te(IV) removal (89 - 95%) is, however, slightly higher for the experiments at pH 7 than for experiments conducted at pH 9 which show Te removal between 69 – 74% by the end of the experiment (70 hours). The reaction kinetics conform to a first-order rate law $\frac{d[Te(IV)]}{dt} = -k\,[Te(IV)]$ where k is the first-order rate constant for Te(IV). After integrating and linearizing the first-order rate law equation we plotted the experimental data in graphs of ln[Te(IV)] vs t, and determined the first-order rate constants from the slope of the best-fit line via linear regression (Figure 2). There is no evidence of any change of the first-

order reaction rate constant during the course of an experiment. Te(IV) removal rates vary between the experiments with varying initial Te(IV) and between pH conditions.

The first order rate constants of Te(IV) removal decrease with increasing Te(IV) concentration. Low initial Te(IV) concentrations (2 mg L^{-1}) result in 2 to 3.5 times higher *k* compared to that for the high Te concentration (10 mg L^{-1}). This is somewhat counterintuitive because a decrease in initial Te(IV) is not expected to increase the rate constants of first-order reactions. We surmise that the observed anticorrelation between the rate-constants and Te(IV) concentrations arises when Te(IV) at higher concentrations partially passivates the reactive mineral surfaces and slows further surface-mediated reactions. This is caused by the greater depletion of Fe^{2+} on the siderite surface and the formation of magnetite (Fe_3O_4) at higher Te(IV) concentrations. Similar observations have been reported for the interaction between other minerals and metal anions such as sorption-reduction of Cr(VI) by magnetite (Peterson et al., 1997) and siderite (Bibi et al., 2018) as well as sorption-oxidation of Se(IV) by birnessite (Li et al., 2021). We also assume that the particle surface area did not change significantly between the experiments because of an identical amount of injected siderite in each experiment and the uniform particle size of synthesized siderite (Koo and Kim, 2019).

Similarly, Te(IV) removal rates decrease with increasing pH. At similar initial Te(IV) concentration, the reaction rates are 2.7 to 4.8 times higher at pH 7 than at pH 9 (Figure 2 and 3). The inverse relationship between the rate-constants and pH is also related to the surface properties of siderite. The pH of the point of zero charge is 5.5 (Charlet et al., 1990) causing the net surface charge of the siderite surfaces to be negative under our experimental conditions. The negatively charged mineral surface repels Te(IV) anions and slows interaction with the mineral surface. At pH 9, this effect intensifies and slows the surface-mediated reaction down. A similar observation of pH dependence has been reported for Se(IV) and U(VI) adsorption on mineral phases (Badaut et al., 2012; Fox et al., 2006). Despite a net negative charge, sorption of Te(IV) anions still occurs at available positively charged surface sites. This phenomenon is similar to U(VI) adsorption on quartz, where ~90% of U(VI) anionic complexes strongly sorb on to quartz surfaces despite at pH 7.0 (Fox et al., 2006) despite a net negative surface

charge because the point of zero charge for quartz is 2.0 (Kosmulski, 2002). These results show that pH plays an important role in controlling the surface-mediated Te(IV) removal from solution over time.

3.2 Redox reaction. On siderite surfaces, Te(IV) is reduced to Te(0) coupled to oxidation of Fe(II) in siderite to Fe(III) resulting in magnetite formation. The mineralogical transformation is evident from the change of grey colored siderite to a brownish to black magnetic suspension in all batch reactors (Figure S 1). XRD results confirm the formation of elemental Te and magnetite as the mineral product of siderite oxidation (Figure 5). This is similar to Se(IV) reduction, where XANES data showed formation of magnetite for siderite reduction experiments at pH 8 (Scheinost and Charlet, 2008). SEM-EDS results further show surface-mediated reactions and transformation of mineral surface (Figure S2 and S3). The surface contains less carbon and more oxygen (1:5) than the stoichiometric ratio of siderite (1:3) indicating oxidation of siderite to an iron oxide mineral phase (Figure S2). We propose the following reaction for Te(IV) reduction by siderite:

$$6FeCO_3 + TeO_3^{2-} + 5H_2O \rightarrow 2Fe_3O_4 + Te + 10H^+ + 6CO_3^{2-}$$

Once the electron transfer from the surfaces is complete, the siderite surfaces host magnetite, which is composed of mixed Fe(II) – Fe(III) phases and may have the electron donating capacity to reduce Te(IV). Therefore, it needs to be tested whether magnetite is capable of reducing and adsorbing Te(IV) to a similar extent as siderite. We expect that Te(IV) reduction by magnetite is slower because much less Fe(II) is available as electron donor. The proposed reaction suggests that 6 moles of siderite is required to reduce each mole of Te(IV) [i.e., siderite:Te(IV) = 6:1]. In experiments with the highest Te(IV), each reactor contained approximately 0.5 mg (or 3.92 µmol) of Te(IV) and 44.9 mg (or 387.1 µmol) of siderite. Thus, each reactor contains excess reductant to completely reduce the amount of Te(IV) present. However, our results suggest that Te(IV) removal from the solution is due to both adsorption and reduction of Te(IV) on siderite surfaces (see below).

3.3 Reaction mechanism. Based on the results described above, we propose that reduction of Te(IV) by siderite is a two-step reaction on the mineral surface under the tested experimental conditions. Immobilization of Te(IV) by siderite most likely follows the same surface-mediated reactions, which

have been observed for Se(IV) (Scheinost and Charlet, 2008; Badaut et al., 2012). At first, Se(IV) is immobilized on the siderite surface via adsorption before being reduced to Se(0) (Badaut et al., 2012). Similarly, a recent work (Yu et al., 2018) has shown adsorption of Te(IV) on nanoscale zero-valent iron (ZVI) prior to reduction to Te(0) on zero-valent iron surfaces. Here, we hypothesize that Te(IV) is first retained at the siderite surface by formation of surface complexes, and then reduced to Te(0) after interfacial electron transfer. This is supported by several lines of evidence. First, the lack of any deviation from the first-order reaction rate in each experiment indicates a single mechanism for removal of Te(IV) from solution. A single rate-constant would not fit the data from our experiment if multiple mechanisms (both adsorption and reduction) were simultaneously removing Te(IV) from the solution. Second, removal of [Te(IV)] is followed by the formation of the reaction products, elemental Te and magnetite, which clearly demonstrate interfacial electron transfer. This interfacial electron transfer would be facilitated by the formation of Fe-Te inner-sphere complexes. Studies on chemically similar Se(IV) and its reduction by siderite showed that ~72% of the adsorbed Se(IV) was reduced to Se(0) on the siderite surface and it has been argued that adsorption of Se(IV) and subsequent reduction to Se(0) was the primary mechanism of Se(IV) removal in siderite experiments (Badaut et al., 2012). Our isotope results test the hypothesis and provide valuable insights into the mechanisms of Te(IV) removal and reduction by siderite.

3.4 Tellurium isotope fractionation. Measurable Te isotopic fractionation is observed in each reactor (Figure 4). While Te(IV) in solution decreases, the δ^{130}Te values of the remaining Te(IV) increase systematically. In these well-mixed batch reactors, the isotopic fractionation can be described by the Rayleigh distillation models assuming a potentially irreversible reaction that removes Te from the solution. The magnitude of Te isotopic fractionation (as ε) obtained by fitting δ^{130}Te data to Eq. 3 are illustrated in Figure 4 and summarized in Table S1. The ε^{130}Te values range between –0.10‰ and –0.26‰. The two- to three-fold change in first-order rate constants between pH's and initial Te(IV) concentrations (Figure 2 and 3), only induce negligible difference in Te isotope fractionation.

Small Te isotopic fractionation, as observed in our experiments, confirms that Te(IV) removal from the solution is largely controlled by adsorption of Te(IV) on to available surface sites of siderite. Tellurium isotope fractionation for biotic and abiotic reduction of Te(IV) is an order of magnitude larger than the observed ε in our experiments ($\varepsilon^{130/125}$Te = –0.23 ± 0.06‰, Table 1). Reduction of Te(IV) by *Bacillus selenitireducens* yielded an isotope fractionation of –4.0‰ (Baesman et al., 2007). The Te isotope fractionation by siderite is also an order of magnitude smaller than ε values reported for Te(IV) reduction by dissolved cysteine ($\varepsilon^{130/125}$Te = –2.35‰) (Baesman et al., 2007) and sulfite ($\varepsilon^{130/125}$Te = –4.4‰) (Smithers and Krouse, 1968) (Table 1). If reduction determined the isotope fractionation for the reaction of Te(IV) with siderite, we would observe a much larger isotopic fractionation, on the order of several per mil, because of large changes in the bonding environment of Te.

The mechanism of the immobilization of Te(IV) onto the siderite surface determines the magnitude of Te isotope fractionation. Reduction of Te(IV) involves breakage of Te–O bonds and large changes in the coordination of oxygens around Te atoms. This rearrangement of Te–O bonds favors lighter isotopes and would be expected to result in a large isotopic fractionation (Schauble et al., 2004). If Te(IV) reduction were the dominant fractionating mechanism, a large fractionation up to several per mil would be observed in the Te isotope ratios of the reactant. In contrast, the adsorption of Te(IV) requires much smaller changes in the bonding environment of Te (Tucker et al., 1962). So, if adsorption of Te(IV) is the dominant fractionating mechanism, it produces a smaller isotopic fractionation than that for reduction reactions. Although both adsorption and reduction are at work in our experiments, adsorption occurs first followed by reduction. For strong sorption which is not fully reversible, the sorbed Te(IV) pool is in limited chemical communication or exchange with the dissolved Te(IV). This limitation of chemical and therefore, isotopic exchange effectively sequesters surficial Te(IV) reduction and concomitant large isotopic fractionation from the dissolved Te(IV). Similar isolation of reduction from the bulk reactant pool produces diminished U isotopic fractionation during bacterial U(VI) reduction (Basu et al., 2020).

Adsorption of Te(IV) onto siderite appears to control the magnitude of isotope fractionation ($\varepsilon^{130/125}$Te = –0.23 ± 0.06‰) observed in our experiments, and therefore, we infer that adsorption is determines the extent of isotope fractionation for the overall adsorption-reduction process. The small ε values for Te(IV) are similar to isotope fractionations of other oxyanions by adsorption on various mineral phases. For example, adsorption of Se(IV) on iron (oxy)hydroxide causes similar small fractionation ($\varepsilon^{82/76}$Se = <1‰) (Mitchell et al., 2013, Xu et al., 2020). Within the tested pH range, we assume that adsorbed Te(IV) ions likely form stable inner sphere complexes that remain strongly attached to the surfaces prior to electron transfer (Harada and Takashi, 2008; Kashiwabara et al., 2014). Sorption of Te(IV) leads to a sequestration of Te(IV) from the solution that results in a lack of mixing between the adsorbed and dissolved reactants. Adsorbed Te anions undergoing reduction do not affect the isotopic composition of the Te(IV) in solution because none of them can back react to become dissolved Te(IV). Accordingly, even though the reduction step almost certainly fractionates Te isotopes, that effect is not manifested in remaining Te(IV) in solution. Furthermore, the conservation of isotopes requires that the reaction product is not highly fractionated.

4. Environmental implications

Our experiments demonstrate that Te(IV) is efficiently immobilized by siderite under mildly reducing ferruginous conditions at environmental pH (7 – 9). This is relevant for both natural attenuation and active remediation sites undergoing engineered interventions. Under ferruginous conditions in soils and aquifers, siderite can be formed as a byproduct of microbial Fe(II) reduction (Jensen et al., 2002; Lin et al., 2020) or as a corrosion product in zero-valent iron permeable reactive barriers (Roh et al., 2000; Lee and Wilkin, 2010). For instance, anoxic, carbonate-bearing groundwater is often supersaturated with respect to the siderite ($K_{sp} = 10^{-10.7}$) (Lee and Wilkin, 2010). Adsorption and reduction of Te can be considered as a naturally occurring immobilization process leading to Te enrichment under ferruginous conditions. Under oxic condition Te(IV) is preferentially adsorbed on iron-hydroxides (Qin et al., 2017, Hayes and Ramos, 2019), and thus any Te(IV) reduction in terrestrial environments should be distinguishable from adsorption reactions by its characteristically large Te isotope fractionation.

Generally, analogous Se(IV) reduction to Se(0) by siderite is rapidly promoted in oxygen-depleted environments such as at nuclear waste disposal sites due to low solubility of siderite (Badaut et al., 2012). Our results suggest that these conditions should also create a sink for Te that can be applied to Te removal from wastewater.

5. Future work

Our study lays the necessary foundations for future Te isotope analysis and demonstrates the relevance of determining the extent of isotope fractionation experimentally prior studying complex environmental systems. The isotopic composition of the major Te sources must be characterized and fractionation factors for the principal reactions occurring in the in waters, atmosphere and soils need to be determined. Although our experiments tested siderite at neutral–mildly basic conditions, several other chemical conditions may be determined to provide a broader picture of Te isotope fractionation during reduction and/or adsorption. Future studies should explore Te isotope fractionation during mineral interaction causing reduction or adsorption of either of Te(IV) or Te(VI). The small size of isotopic fractionation in our experiments could occur if reduction of Te(IV) by siderite produced a smaller fractionation intrinsic to the reduction reaction. However, two studies on abiotic Te reduction (Smithers and Krouse, 1968; Baesman et al., 2007) show much larger fractionations and thus we suggest this is unlikely. Future experimental work could explore this idea more by measuring isotopic fractionation induced by Te(IV) reduction by siderite, under conditions where the effect of adsorption is minimized due to presence of anions such as phosphate competing for the available surface sites (i.e., higher ionic strength).

Furthermore, adsorption of Te(IV) and Te(VI) to Fe(III)oxy-hydroxides is a common pathway in oxic soils, so investigating the isotopic behavior of adsorbed Te may be helpful in better understanding soil cycling and bioavailability of Te. Further, studying Te isotope fractionation by adsorption of Te(IV) and Te(VI) to clay minerals would be important to differentiate Te sequestration between Fe(III) hydroxide and clay minerals. If we develop well-constraint isotope fractionation factors experimentally then Te stable isotope measurement can provide important insights into the sources, transformation and deposition of Te.

5. Acknowledgement

We thank Phil Holdship at the Department of Earth Sciences, Oxford University for his help in the Te concentration measurement on the ICP-MS. We thank Sharon Gibbons for helping with SEM analysis and James Brakeley for helping with XRD measurements at the Department of Earth Sciences, Royal Holloway, University of London. This research was financially supported by the Royal Society and the Hester Cordelia Fund, Oxford University (HCF/HT2018).

6. Contribution

A.B. and K.S. designed the study and conducted the experiments. N.W. conducted the Te isotope analysis; and all authors contributed to writing the manuscript.

References:

Badaut V., Schlegel ML., Descostes M., Moutiers G. 2012. In situ time-resolved X-ray near-edge adsorption spectroscopy of selenite reduction by siderite. Environ. Sci. Technol. 48, 10820–10826.

Baesman S.M., Bullen T.D., Dewald J., Zhang, D., Curran S., Islam F.S., Beveridge T.J., Oremland R.S. 2007. Formation of tellurium nanocrystals during anaerobic growth of bacteria that use Te oxyanions as respiratory electron acceptors. Appl. Environ. Microbiol. 73, 2135–2143.

Basu A., Schilling K., Brown S.T., Johnson T.M., Christensen J.N., Harmann M., Reimus P.W., Heikoop J.M., Woldegabriel G., DePaolo D.J. 2016. Se isotopes as groundwater redox indicator: Detecting natural attenuation of Se at an in-situ recovery U mine. Environ. Sci. Technol. 50, 10833–10842.

Basu A., Johnson T.M. 2012. Determination of hexavalent chromium reduction using Cr stable isotopes: Isotopic fractionation factors for permeable reactive barrier materials. Environ. Sci. Technol. 46, 5353–5360.

Bibi I., Niazi N.K., Choppala G., Burton E.D. 2018. Chromium(VI) removal by siderite ($FeCO_3$) in anoxic aqueous solutions: An X-ray adsorption spectroscopy investigation. Sci. Tot. Environ. 640-641: 1424-1431.

Charlet L., Wersin P., Stumm W. 1990. Surface charge of $MnCO_3$ and $FeCO_3$. Geochim. Cosmochim. Acta 54, 2329–2336.

Clark S.K., Johnson T.M. 2010. Selenium stable isotope investigation into selenium biogeochemical cycling in a lacustrine environment: Sweitzer Lake, Colorado. J. Environ. Qual. 39, 2200–2210.

Doulgeridou, A., Amlund H., Sloth JJ., Hansen M. Review of potentially toxic rare earth elements, thallium and tellurium in plant-based food. EFSA Journal 18(1): e181101.

Fehr M.A., Hammond S.J., Parkinson I.J. 2018. Tellurium stable isotope fractionation in chondritic meteorites and some terrestrial samples. Geochim. Cosmochim. Acta 222, 17–33.

Fehr, M.A., Rehkämper, M., Halliday, A.N., Schönbächler, M., Hattendorf, B., Günther, D. 2006. Search for nucleosynthetic and radiogenic tellurium isotope anomalies in carbonaceous chondrites. Geochim. Cosmochim Acta 70(13), 3436-3448.

Filella, M; May, P.M 2019. The aqueous chemistry of tellurium: critically-selected equilibrium constants of the low-molecular-weight inorganic species. Environ. Chem. 16(4), 289-295.

Fornadel, A.P., Spry, P.G., Haghnegahdar, M.A., Schauble, E.A., Jackson, S.E., Mills, S.J. 2017. Stable Te isotope fractionation in tellurium-bearing minerals from precious metal hydrothermal ore deposits. Geochim. Cosmochim. Acta 202, 215-230.

Fornadel, A.P., Spry, P.G., Jackson, S.E. 2019. Geological controls on the stable tellurium isotope variation in tellurides and native tellurium from epithermal and orogenic gold deposits: Application to the Emperor gold-telluride deposit, Fiji. Ore Geol. Rev. 113, 103076.

Fox, P. M., Davis, J. A., Zachara, J. M. 2006. The effect of calcium on aqueous uranium U(VI) speciation and adsorption to ferrihydrite and quartz. Geochim. Cosmochim. Acta. 70, 1379-1387.

Fukami, Y., Kashiwabara, T., Amakawa, H., Shibuya, T., Usui, A., Suzuki, K. 2022. Tellurium stable isotope composition in the surface layer of ferromanganese crusts from two seamounts in the Northwest Pacific Ocean. Geochim. Cosmochim. Acta 318, 279-291.

Gil-Díaz T., Schäfer J., Dutruch L., Bossy C., Pougnet F., Abdou M., Lerat-Hardy A., Pereto C., Derriennic H., Briant N., Sireau T., Knoery J., Blanc. 2019. Tellurium behaviour in a major European fluvial–estuarine system (Gironde, France): fluxes, solid/liquid partitioning and bioaccumulation in wild oysters. Environ. Chem. 16: 229-242.

Harada T., Takahashi, Y. 2008. Origin of the difference in the distribution behavior of tellurium and selenium in a soil-water system. Geochim. Cosmochim. Acta 72, 1281–1294.

Hayes S.M., McCullough E.A. 2018. Critical minerals: A review of elemental trends in comprehensive critically studies. Resour. Pol. 59, 192–199.

Hayes S.M., Ramos N.A. 2019. Surficial geochemistry and bioaccessibility of tellurium in semiarid mine tailing. Environ. Chem. 16, 251–265.

Hein J.R., Koschinsky, A., Halliday A.N. 2003. Global occurrence of tellurium-rich ferromangenese crusts and a model for the enrichment of tellurium. Geochim. Cosmochim. Acta 67, 1117–1127.

Hellmann J.L., Hopp T., Burkhardt C., Becker H., Fischer-Gödde, Kleine T. 2021. Tellurium isotope geochemistry: Implications for volatile fractionation in chondrite parent bodies and origin of the late veneer. Geochem. Cosmochim Acta 309, 313-328.

Ithurbide A., Peulon S., Miserque F., Beaucaire C., Chausse A. 2009. Interaction between uranium (VI) and siderite (FeCO3) surfaces in carbonate solutions. Radiochim. Acta 97, 177–180.

Jensen D.L., Boddum J.J., Tjell J.C., Christensen T.H. 2002. The solubility of rhodochrosite ($MnCO_3$) and siderite ($FeCO_3$) in anaerobic aquatic environments. Appl. Geochem. 17, 503–511.

Kashiwabara T., Oishi Y., Sakaguchi A., Sugiyama T., Usui A., Takahashi Y. 2014. Chemical processes for the extreme enrichment of tellurium into marine ferromanganese oxides. Geochim. Cosmochim. Acta 131, 150–163.

Kaufman A.J., Hayes J.M., Klein C. 1990. Primary and diagenetic controls of isotopic compositions of iron-formation carbonates. Geochim. Cosmochim. Acta 54, 3461–3473.

Kavlak, G., Graedel, T.E. 2013. Global anthropogenic tellurium cycles for 1940−2010. Resour. Conserv. Recycl. 76, 21−26.

Kessi J., Turner R.J., Zannoni D. 2022. Tellurite and selenite: how can these two oxyanions be chemically different yet so similar in the way they are transformed to their metal forms by bacteria? Biol Res. 5 55(1):17

Kim J.D., Yee N., Nanda V., Falkowski P.G. 2013. Anoxic photochemical oxidation of siderite generates molecular hydrogen and iron oxides. Proc. Nat. Sci. Ac. 110, 10073–10077.

Koo, T. and Kim, J. 2019. Controls on the formation and stability of siderite ($FeCO_3$) and chukanovite ($Fe(CO_3)(OH)_2$) in reducing environment. Minerals. 10(2), 156, doi:10.3390/min10020156.

Kosmulski, M. 2002. The pH-dependent surface charging and points of zero charge. J. Colloid Interface Sci. 253, 77-87.

Lee T.R., Wilkin R.T. 2010. Iron hydroxy carbonate formation in zerovalent iron permeable reactive barriers: Characterization and evaluation of phase stability. J. Contamin. Hydrol. 116, 47–57.

Legrand L., El Figuigui A., Mercier F., Chausse A. 2004. Reduction of aqueous chromate by Fe(II)/Fe(III) carbonate green rust: kinetic and mechanistic studies. Environ. Sco. Technol. 38(17): 4587-4595.

Li Z., Yuan Y., Ma L., Zhang Y., Jiang H., He J., Yuan S., Ginder-Vogel M., Tu S. 2021. Simultaneous kinetics of selenite oxidation and sorption on δ-MnO_2 in stirred reactors. Int. J. Environ. Res. Public Health. 18(6): 2902.

Lin C.Y., Turchyn A.V., Krylov A., Antler G. 2020. The microbially driven formation of siderite in salt marsh sediments. Geobiol. 18, 207–224.

Missen, O.P., Ram, R., Mills, S.J., Etschmann, B., Reith, F., Shuster, J., Smith, D.J., Brugger, J. 2020. Love is in the Earth: A review of tellurium (bio)geochemistry in surface environments. Earth-Science Reviews. 204, 1031350.

Missen, O.P., Lausberg, E.R., Brugger J., Etschmann B., Mills, S.J., Momma, K., Ram, R., Maruyama, M., Fang, X.Y., Melchiorre, E., Ryan, C.G., Villalobos-Portillo, E.E., Castillo-Michel, H., Nitta, K., Sekizawa, O., Shuster, J., Sanyal, S.K., Frierdich, A., Hunt, S., Tsuri, Y., Takahashi, Y., Michibata, U., Dwivedi, S., Rea, MA.D. 2022. Natural nanoparticles of the critical element tellurium, J. Hazard. Mat. Lett. 3" 100053.

Mitchell K., Couture R.M., Johnson T.M., Mason P.R.D., Van Cappellen P. 2013. Selenium sorption and isotope fractionation: Iron(III) oxides versus iron(II) sulfides. Chem. Geol. 342, 21–23

Moreno T., Oldroyd A. McDonald I., Gibbons, W. 2007. Preferential fractionation of trace metals-metalloids into PM10 resuspended from contaminated gold mine tailings at Rodalquilar, Spain. Wat. Air Soil Poll. 179, 93–105.

Perkins W.T. 2011. Extreme selenium and tellurium contamination in soils — An eighty-year-old industrial legacy surrounding a Ni refinery in the Swansea Valley. Sci. Tot. Environ. 412-413, 162–169.

Peterson M.L., White A.F., Brown G.E., Parks G.A. 1997. Surface passivation of magnetite by reaction with aqueous Cr(VI): XAFS and TEM. Environ. Sci. Technol. 31(5): 1573-1576.

Qin, H-B., Takeichi Y., Nitani H., Terada Y., Takahashi, Y. 2017. Tellurium distribution and speciation in contaminated soils from abandoned mine tailings: Comparison with selenium. Environ. Sci. Technol. 51, 6027–6035.
Rakshit S., Matocha C.J., Coyne M.S. 2008. Nitrite reduction by siderite. Soil Sci. Soc. Am. J. 72, 1070–1077.
Ramos-Ruiz A., Field J.A., Wilkening J.V., Sierra-Alvarez R. 2015. Recovery of elemental tellurium nanoparticles by the reduction of tellurium oxyanions in a methanogenic microbial consortium. Environ. Sci. Technol. 50, 1492–1500.
Rees C.E. 1973. A steady-state model for sulphur isotope fractionation in bacterial reduction processes. Geochim. Cosmochim Acta 37, 1141–1162.
Reinhard C.T., Planavsky N.J., Wang X., Fischer W.W., Johnson T.M., Lyons T.W. 2014. The isotopic composition of authigenic chromium in anoxic marine sediments: A case study from the Cariaco Basin. Earth Planet. Sci. Lett. 407, 9–18.
Rietveld H.M. 1969. A profile refinement method for nuclear and magnetic structures. J. Appl. Cryst. 2, 65–71.
Roh Y., Lee S.Y., Elless M.P. 2000. Characterization of corrosion products in the permeable reactive barriers. Environ. Geochem. 40, 184–194.
Ruiz-de-Cenzano M., Rochina-Marco A., Cervera M.L., de la Guardia M. 2017. Evaluation of the content of antimony, arsenic bismuth, tellurium and their inorganic forms in commercially baby food. Biol. Trac. Elem. Res. 180: 355-365.
Schauble E.A. 2004. Applying stable isotope fractionation theory to new systems. Rev. Mineral. Geochem. 55: 65-111.
Scheinost A.C., Charlet L. 2008. Selenite reduction by mackinawite, magnetite and siderite: XAS characterization of nanosized redox products. Environ. Sci. Technol. 42, 1984–1989.
Schilling K., Johnson T.M., Dhillon K.S., Mason P.R.D. 2015. Fate of selenium in soils at a selenifeorus site recorded by high precision Se isotope measurements. Environ. Sci. Technol. 49, 9690–9698.
Smithers R.M., Krouse H.R. 1968. Tellurium isotope fractionation study. Can. J. Chem. 46(4), 583–591.
Sovacool, B. K., Ali, S. H., Bazilian, M., Radley, B., Nemery, B., Okatz, J., Mulvaney, D. 2020. Sustainable minerals and metals for a low-carbon future. Science, 367 (6473), 30-33.
Talens Peiro L., Villaba Mendez G., Ayres R.U. 2013. Material flow analysis of scare metals: Sources, functions, end-uses and aspects for future supply. Environ. Sci. Technol. 47, 2939–2947.
Taylor, D.E. 1999. Bacterial tellurite resistance, Trends Microbiol. 7(3): 111-115.
Tucker F.L., Walper J.F., Appleman M.D., Donohue, J. 1962. Complete reduction of tellurite to pure tellurium metal by microorganisms. J. Bacteriol. 83, 1313–1314.
US Department of the Interior. 2022. Final List of Critical Minerals 2022. Federal Register 87, no. 37. https://www.govinfo.gov/content/pkg/FR-2022-02-24/pdf/2022-04027.pdf
Vij P., Hardej D. 2016. Alterations in antioxidant/oxidant gene expression and proteins following treatment of transformed and normal colon cells with tellurium compounds. Environ. Toxicol. Phamacol. 43, 216–224.
Wasserman N.L., Johnson T.M. 2020. Measurements of mass-dependent Te isotopic variation by hydride generation MC-ICP-MS. J. Anal. At. Spectrom. 35, 307–319.
Wasserman, N.L., Mackinney, J., & Johnson, T. M. (2017) Antimony and tellurium stable isotopes as redox indicators in surface environments. Paper presented at the 12th International Symposium on Applied Isotope Geochemistry (AIG-12), Copper Mountain, CO, 2017
Watari T., McLellan B.C., Ogata S., Tezuka T. 2018. Analysis of potential for critical metal resource constrains in the international energy agency's long-term low-carbon energy scenarios. Minerals 8, 156
Watari T., Nansai, K., Nakajima K. 2020. Review of critical metal dynamics to 2050 for 48 elements. Resour. Conserv. Recycl. 155, 104669
Wei W., Klaebe R., Ling H.F., Huang F., Frei R. 2020. Biogeochemical cycle of chromium isotopes as the modern Earth's surface and its applications as a paleo-environment proxy. Chem. Geol. 541, 119570.

Wiesli R.A., Beard B.L., Tobschall H.J. 2004. Experimental determination of Fe isotope fractionation between aqueous Fe(II), siderite and "green rust" in abiotic systems. Chem. Geol. 211, 343–362.

Wiklund J.A., Kirk J.L., Muir D.c.G., Carrier J., Gleason A., Yang F., Evans M., Keating J. 2018. Widespread atmospheric tellurium contamination in industrial and remote regions of Canada. Environ. Sci. Technol. 52(11): 6137-6145.

Wray D.S 1998. The impact of unconfined mine tailings and anthropogenic pollution on a semi-arid environment–An initial study of the Rodalquilar mining district, southeast Spain. Environ. Geochem. Health 20, 29–38.

Xu W., Zhu J.M., Johnson T.M., Wang X., Lin Z.Q., Tan D., Qin H. 2020. Selenium isotope fractionation during adsorption by Fe, Mn and Al oxides. Geochim. Cosmochim. Acta 272, 121–136.

Yarema M.C., Curry S.C. 2005. Acute tellurium toxicity from ingestion of metal-oxidizing solutions. Pediatrics 116, 319–321.

Yu H., Chu Y., Zhang T., Yu L., Yang D., Qiu F., Yuan D. 2018. Recovery of tellurium from aqueous solutions by adsorption with magnetic nanoscale zero-valent iron (NZVFe) Hydrometal. 177, 1–8.

Zannoni D., Borsetti F., Harrison J.J., Turner R.J. 2007. The bacterial response to the chalogen metalloids Se and Te. Adv. Microb. Physiol. 53, 1–7.

Zhu J.M., Johnson T.M., Clark S.K., Zhu X.K., Wang Z.L. 2014. Selenium redox cycling during weathering of Se-rich shales: A selenium isotope study. Geochim. Cosmochim. Acta 126, 228–249.

Figures

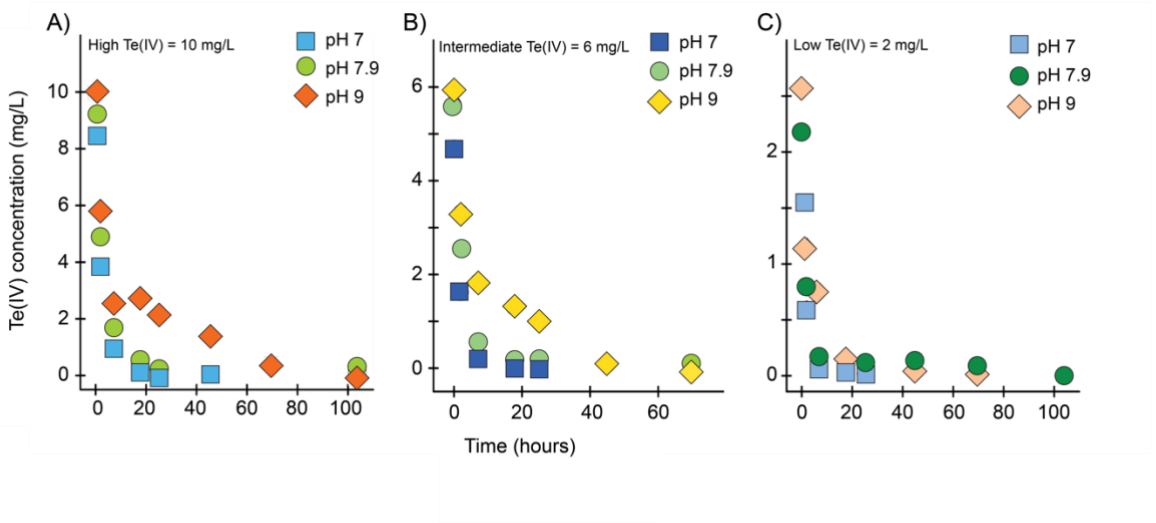

Figure 1: Te(IV) removal by siderite. Decrease of Te(IV) in solution with time for A) high B) intermediate and C) low Te concentration at pH 7, 7.9 and 9.

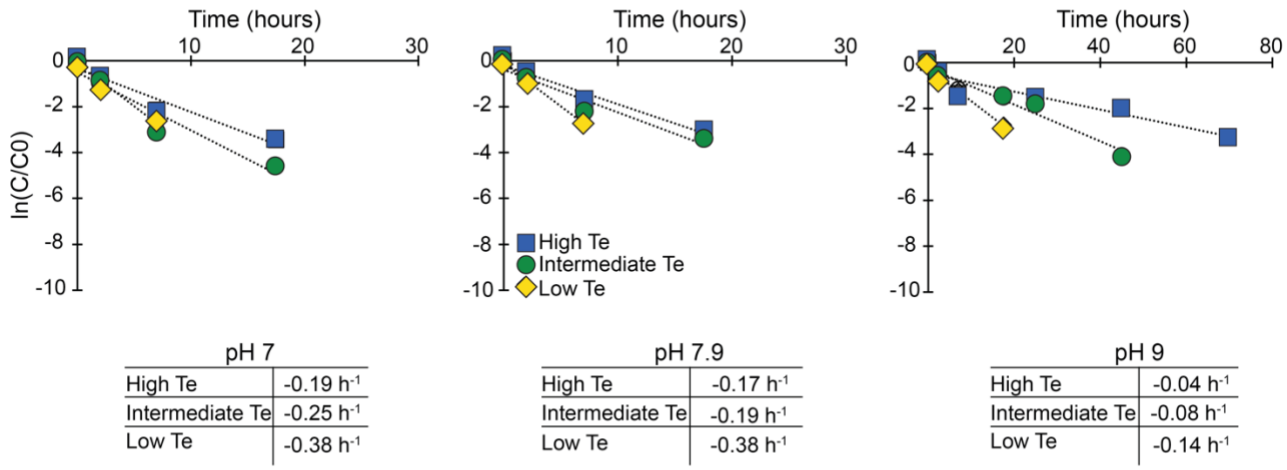

Figure 2: First-order rate constants of Te(IV) immobilization by siderite as a function of concentration low (2 mg L^{-1}), intermediate (6 mg L^{-1}), and high Te (10 mg L^{-1}).

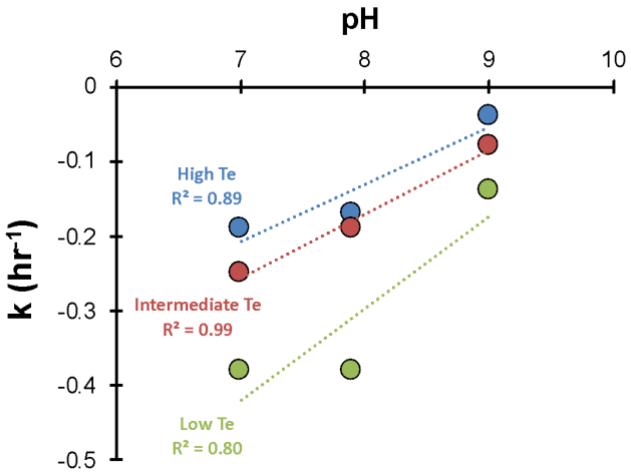

Figure 3: First-order rate constants of Te(IV) removal/immobilization by siderite as a function of pH for three Te(IV) initial concentrations; low (2 µg mL^{-1}), intermediate (6 µg mL^{-1}), and high Te (10 µg mL^{-1}).

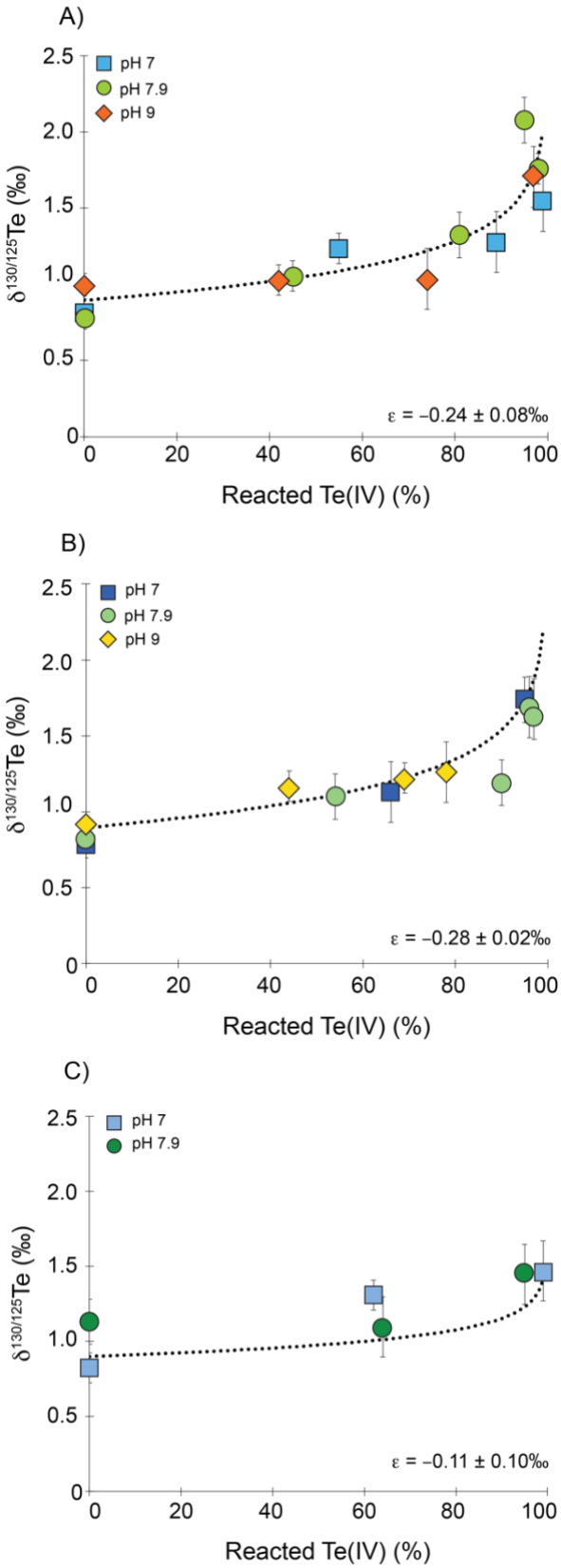

Figure 4: δ^{130}Te (‰) plotted against the fraction of remaining Te(IV) in solution for A) high B) intermediate and C) low Te concentration at pH 7, 7.9 and 9. Lines represent best-fit Rayleigh Models. Error bars represent 2*standard error.

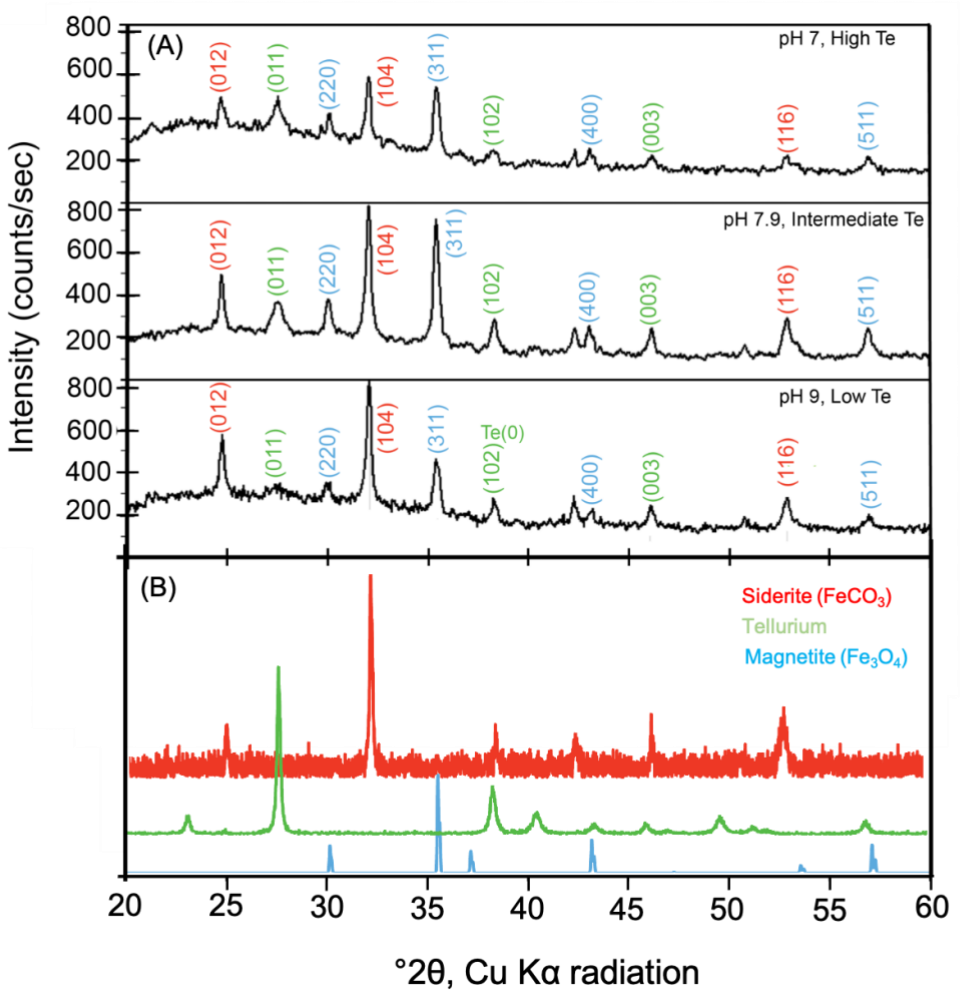

Figure 5: X-ray diffraction (XRD) pattern of the (A) mineral phases after the experiments for three conditions: high Te(IV) at pH 7, intermediate Te(IV) at pH 7.9 and low Te(IV) at pH 9. (B) Reference XRD pattern for siderite (red, R050349), tellurium (green, R070376) and magnetite (blue, R061111) literature.

Table 1: Summary of Te isotope fractionation by biotic and abiotic reductants

Reactant	Oxyanion	Reaction	$\varepsilon^{130/125}$Te (‰)	$\varepsilon^{130/126}$Te (‰)	pH	References
Biotic						
B. selenitireducens	Te(IV)	Reduction	-4.00	-3.2	nd	Baesman et al. (2007)
S. barnesii	Te(VI)	Reduction	-1.95	-1.56	nd	Baesman et al. (2007)
Abiotic						
L-cysteine	Te(IV)	Reduction	-2.35	-1.88	nd	Baesman et al. (2007)
Sulfite	Te(IV)	Reduction	-4.40	-3.52	nd	Smithers & Krouse (1967)
Siderite	Te(IV)	Adsorption	-0.13 to -0.29	-0.1 to -0.23	7	Our study
Siderite	Te(IV)	Adsorption	-0.24 to -0.28	-0.19 to -0.22	7.9	Our study
Siderite	Te(IV)	Adsorption	-0.29 to -0.33	-0.23 to -0.26	9	Our study

nd = not determined

SUPPORTING INFORMATION

Te(IV) immobilization by siderite: Reaction kinetics, mechanism, and Te isotopic fractionation

Anirban Basu[1], Kathrin Schilling[2]*, Alex N Halliday[3], Naomi Wasserman[4], Thomas M. Johnson[5]

[1]*Department of Earth Sciences, Royal Holloway, University of London, Egham, TW20 0EX, United Kingdom*

[2]*Department of Environmental Health Sciences, Columbia University Mailman School of Public Health, New York, NY, USA*

[3]*Earth Institute, Columbia University, New York, NY, USA*

[4]*Nuclear and Chemical Sciences Division, Lawrence Livermore National Laboratory, Livermore, CA 94550, USA*

[5]*Department of Geology, University of Illinois at Urbana-Champaign, Champaign, IL, 61820, USA*

Table S1: Result summary of Te reduction experiments by siderite at low, intermediate and high Te concentrations and three pHs.

	t (hr)	Te(IV) (μg ml^{-1})	Te(IV) Removal	ln[C/C_0]	$\delta^{130/125}$Te (‰)	$\delta^{130/125}$Te (‰)	t (hr)	Te(IV) (μg ml^{-1})	Te(IV) Removal	ln[C/C_0]	$\delta^{130/125}$Te (‰)	$\delta^{130/126}$Te (‰)	t (hr)	Te(IV) (μg ml^{-1})	Te(IV) Removal	ln[C/C_0]	$\delta^{130/125}$Te (‰)	$\delta^{130/126}$Te (‰)
	High Te(IV) concentration						Intermediate Te(IV)						Low Te(IV)					
pH 7	0	8.46	0%	0.000	0.83	0.66	0	4.69	0%	0	0.87	0.70	0	1.56	0%	0	0.83	0.66
	2	3.85	55%	-0.789	1.23	0.99	2	1.62	66%	-1.065	1.13	0.91	2	0.59	62%	-0.974	1.31	1.05
	7	0.97	89%	-2.165	1.28	1.02	7	0.22	95%	-3.052	1.74	1.39	7	0.10	93%	-2.701	na	na
	17.5	0.27	97%	-3.442	na	nd	17.5	0.05	99%	-4.614	na	na	17.5	0.04	97%	-3.643	na	na
	25	0.07	99%	-4.791	1.55	1.24	25	0.01	100%	-5.809	na	na	25	0.02	99%	-4.532	1.47	1.18
	High Te(IV) concentration						Intermediate Te(IV)						Low Te(IV)					
pH 7.9	0	9.15	0%	0	0.81	0.65	0	5.61	0%	0	0.85	0.68	0	2.18	0%	0	1.13	0.90
	2	5.00	45%	-0.604	1.06	0.84	2	2.56	54%	-0.785	1.10	0.88	2	0.79	64%	-1.011	na	0.88
	7	1.71	81%	-1.680	1.32	1.06	7	0.56	90%	-2.313	1.19	0.95	7	0.15	93%	-2.696	na	nd
	17.5	0.44	95%	-3.032	2.08	1.66	17.5	0.19	97%	-3.397	1.68	1.34	25	0.11	95%	-2.966	1.45	1.16
	25	0.24	97%	-3.648	na	nd	25	0.21	96%	-3.268	1.69	1.35	45	0.14	94%	-2.746	na	nd
	103	0.15	98%	-4.141	1.76	1.41	69.7	0.09	98%	-4.108	na	nd	69.7	0.07	97%	-3.497	na	nd
	High Te(IV) concentration						Intermediate Te(IV)						Low Te(IV)					
pH 9	0	9.97	0%	0	0.97	0.78	0	5.92	0%	0	0.80	0.64	0	2.58	0%	0	0.98	0.79
	2	5.80	42%	-0.542	1.03	0.82	2	3.31	44%	-0.582	1.17	0.93	2	1.15	55%	-0.809	na	na
	7	2.56	74%	-1.360	1.04	0.83	7	1.83	69%	-1.176	1.22	0.98	7	0.75	71%	-1.233	na	na
	17.5	2.69	73%	nd	na	nd	17.5	1.32	78%	-1.501	1.26	1.01	17.5	0.17	93%	-2.725	2.08	1.67
	25	2.15	78%	-1.532	na	nd	25	1.01	83%	-1.772	na	nd	45	0.04	98%	-4.051	na	na
	45	1.34	87%	-2.008	1.70	1.36	45	0.10	98%	-4.063	na	nd	69.7	0.00	100%	-7.454	na	na

na = not analyzed

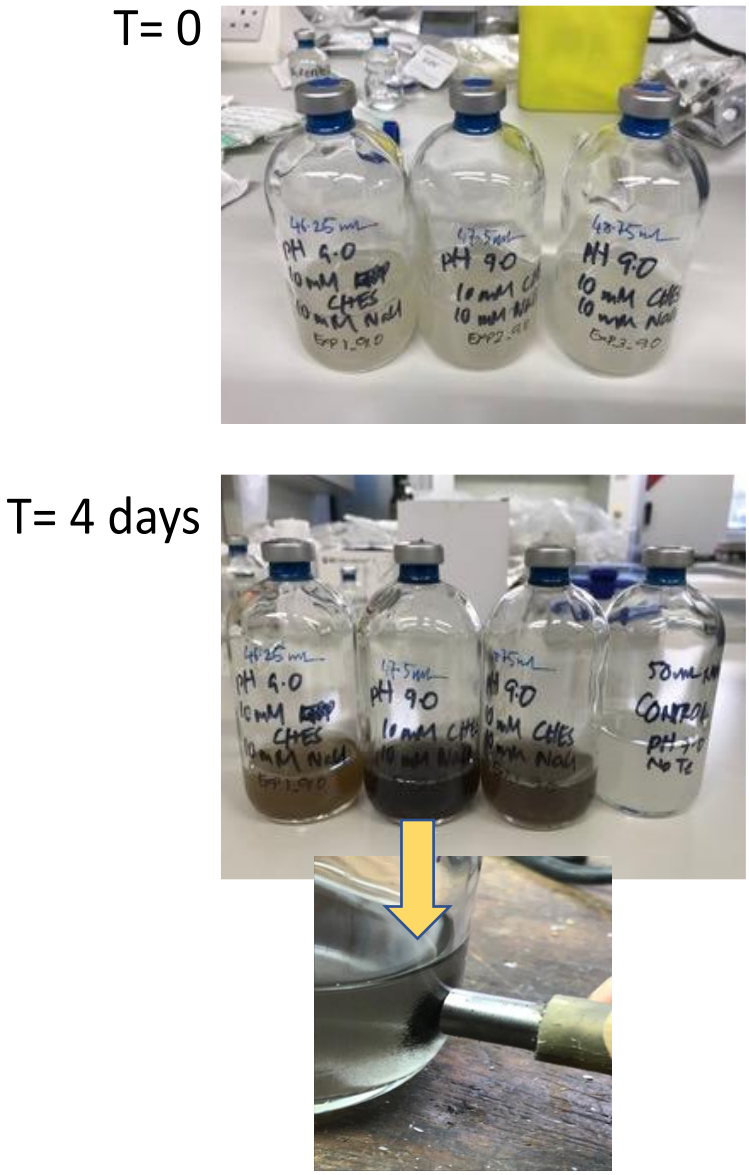

Figure S1: Reduction of Te(IV) by siderite (=reactant) in batch experiments. At the start of the experiments (t=0), the solution is light grey which then turns in to a brownish-black solution after 4 days. The formation of magnetite (=reaction product) with its unique magnetic properties has been proven by an external magnet.

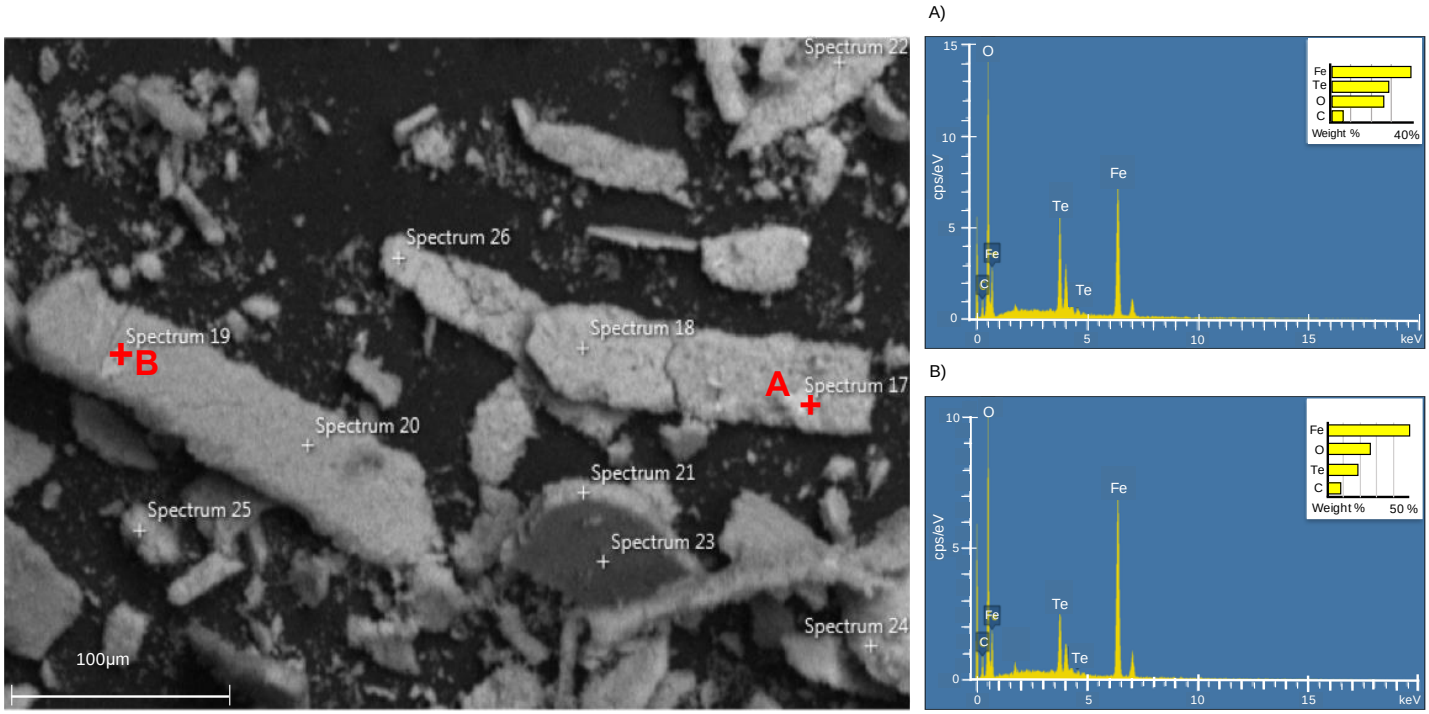

Figure S2: Scanning electron microscopy (SEM) and energy-dispersive X-ray spectroscopy (EDS or EDX) for the siderite with tellurium. (Experiment pH 7)

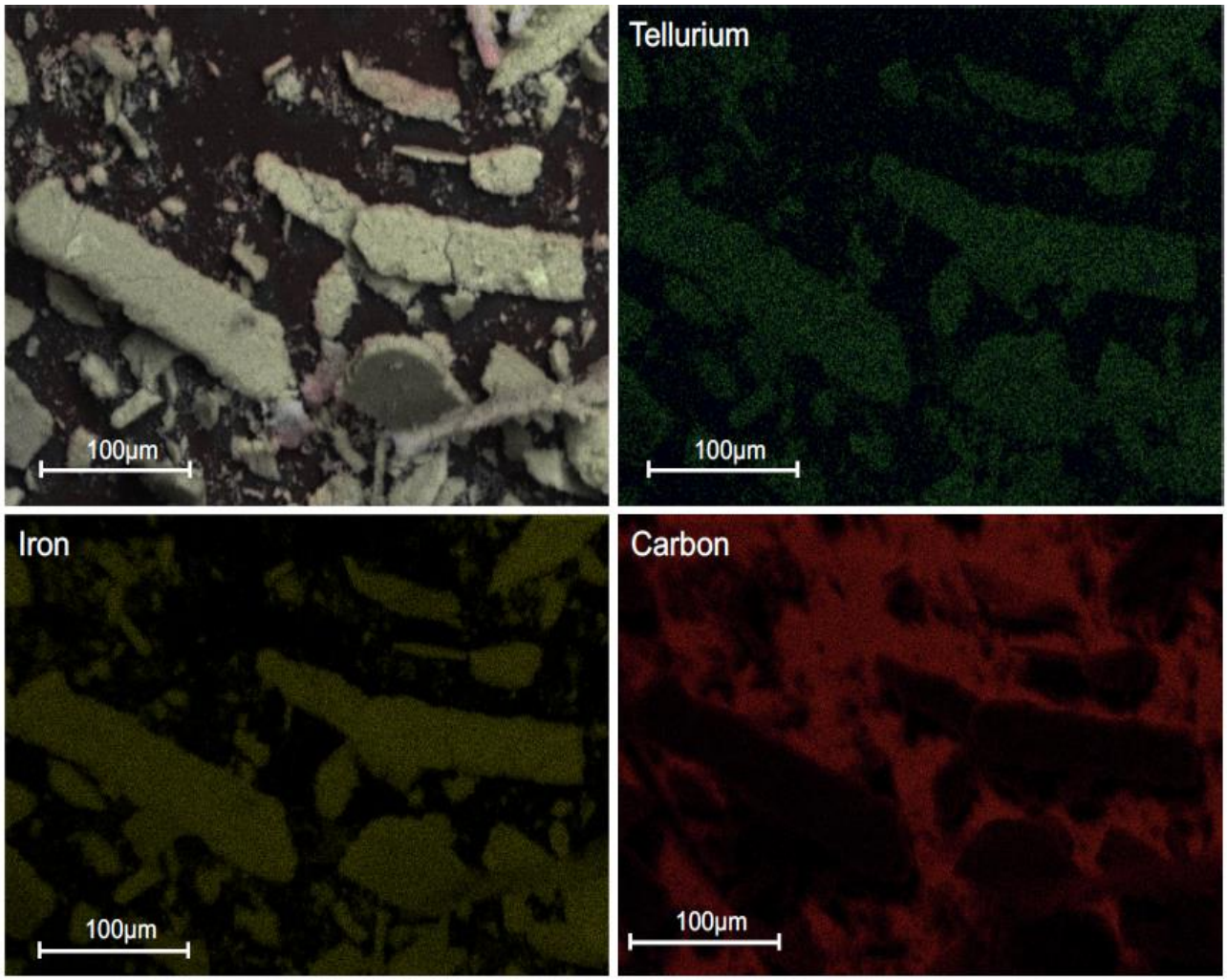

Figure S3: SEM-EDS image and elemental distribution maps of tellurium, iron, and carbon of the reacted siderite (Experiment pH 7)